J|A|C|S
ARTICLES

Published on Web 12/04/2008

The Diels−Alder Reaction on Endohedral $Y_3N@C_{78}$: The Importance of the Fullerene Strain Energy

Sílvia Osuna,[†] Marcel Swart,*[,†,‡] and Miquel Solà*[,†]

Institut de Química Computacional and Departament de Química, Universitat de Girona, Campus Montilivi, 17071 Girona, Catalonia, Spain, and Institució Catalana de Recerca i Estudis Avançats (ICREA), Pg. Lluís Companys 23, 08010 Barcelona, Catalonia, Spain

Received June 25, 2008; E-mail: marcel.swart@udg.edu; miquel.sola@udg.edu

Abstract: We have studied the Diels−Alder reaction of 1,3-butadiene with all nonequivalent bonds of $Y_3N@D_{3h}$-C_{78} at the BP86/TZP//BP86/DZP level of theory. The results obtained are compared with those extracted from a previous study on the free and Sc_3N-endohedral C_{78} fullerene (*J. Am. Chem. Soc.* **2008**, *130*, 6206−6214). Our study shows that the most stable regioisomer for the Y_3N compound is obtained for the reaction over a corannulene-type [5,6] bond (**d**), which exhibits the longest bond distance (1.47 Å) and a large pyramidalization angle. As far as we know, this is the first case of a cycloaddition reaction where the most stable addition is obtained over one of the longest C−C bonds in the cage. In contrast to $Sc_3N@D_{3h}$-C_{78}, where bonds close to the scandium atoms were destabilized, this bond **d** has one of the yttrium atoms in close contact. This preference for reacting with those bonds situated close to the yttrium atoms is due to two different factors: first, the D_{3h} cage is extremely deformed, especially in the areas situated close to the yttrium atoms (which contain the most reactive bond **d**), so the attack reduces the strain energy of the cage; second, in the final adduct, the Y_3N cluster gets additional space to adopt a more planar configuration. Since it has been shown (*J. Phys. Chem. B* **2007**, *111*, 3363−3369) that the D_{3h} isomer is not the most favorable isomer for endohedral $Y_3N@C_{78}$ (at variance with $Sc_3N@C_{78}$), we also studied the more favorable C_2 isomer. The latter contains [5,5] bonds, which are shown to be the most reactive bonds for cycloaddition, in contrast to previous theoretical predictions (*J. Org. Chem.* **2006**, *71*, 46−54). This preference for [5,5] bonds is observed for the C_2 isomers of both endohedral (Sc_3N, Y_3N) and free C_{78} fullerene and is dictated by the fullerene strain energy. We therefore expect that the Diels−Alder reaction on other endohedral metallofullerenes that have already been synthesized (e.g., $Tm_3N@C_2$-C_{78}, $Dy_3N@C_2$-C_{78}) might lead to the same [5,5] adduct.

Introduction

Endohedral metallofullerenes (EMFs) have been intensely studied in recent years because of their potential applications in the fields of biology and medicine as a result of the magnetic, spectroscopic, and nuclear properties of the metal ions encapsulated inside.[1−4] The so-called trimetallic nitride template (TNT) EMFs[5] have attracted increasing attention since 1999, when Dorn and co-workers[6] synthesized for the first time the TNT EMF $Sc_3N@C_{80}$, which is extremely stable and could be obtained in high yields. Other TNT fullerenes, such as $Sc_3N@C_{78}$ and $Sc_3N@C_{68}$, were also obtained[6,7] but in much smaller yields. In these compounds, there exists a formal electronic transfer of six electrons from the M_3N unit to the fullerene structure (M_3N^{6+}:C_x^{6-}). Consequently, the metal cluster encapsulated inside has an enormous influence on the reactivity of these compounds,[3,4] which is, in general, reduced in TNT EMFs as compared with free fullerenes.[8−10] Many recent experimental and theoretical studies have shown that not only the chemical reactivity but also the regioselectivity of TNT EMFs is strongly affected by the encapsulated cluster, metal species, carbon cage size, and symmetry.[1−3,11,12]

[†] Universitat de Girona.
[‡] Institució Catalana de Recerca i Estudis Avançats (ICREA).

(1) Akasaka, T.; Nagase, S. *Endofullerenes: A New Family of Carbon Clusters*; Kluwer Academic Publishers: Dordrecht, The Netherlands, 2002.
(2) Thilgen, C.; Diederich, F. *Chem. Rev.* **2006**, *106*, 5049–5135.
(3) Martín, N. *Chem. Commun.* **2006**, 2093–2104.
(4) Guha, S.; Nakamoto, K. *Coord. Chem. Rev.* **2005**, *249*, 1111–1132.
(5) Kobayashi, K.; Sano, Y.; Nagase, S. *J. Comput. Chem.* **2001**, *22*, 1353–1358.
(6) Stevenson, S.; Fowler, P. W.; Heine, T.; Duchamp, J. C.; Rice, G.; Glass, T.; Harich, K.; Hajdu, E.; Bible, R.; Dorn, H. C. *Nature* **2000**, *408*, 427–428.
(7) Olmstead, M. H.; de Bettencourt-Dias, A.; Duchamp, J. C.; Stevenson, S.; Marciu, D.; Dorn, H. C.; Balch, A. L. *Angew. Chem., Int. Ed.* **2001**, *40*, 1223–1225.
(8) Campanera, J. M.; Heggie, M. I.; Taylor, R. *J. Phys. Chem. A* **2005**, *109*, 4024–4031.
(9) Osuna, S.; Swart, M.; Campanera, J.; Poblet, J.; Solà, M. *J. Am. Chem. Soc.* **2008**, *130*, 6206–6214.
(10) Campanera, J. M.; Bo, C.; Poblet, J. M. *J. Org. Chem.* **2006**, *71*, 46–54.
(11) Cardona, C. M.; Kitaygorodskiy, A.; Echegoyen, L. *J. Am. Chem. Soc.* **2005**, *127*, 10448–10453.
(12) Iiduka, Y.; Ikenaga, O.; Sakuraba, A.; Wakahara, T.; Tsuchiya, T.; Maeda, Y.; Nakahodo, T.; Akasaka, T.; Kako, M.; Mizorogi, N.; Nagase, S. *J. Am. Chem. Soc.* **2005**, *127*, 9965–9957.

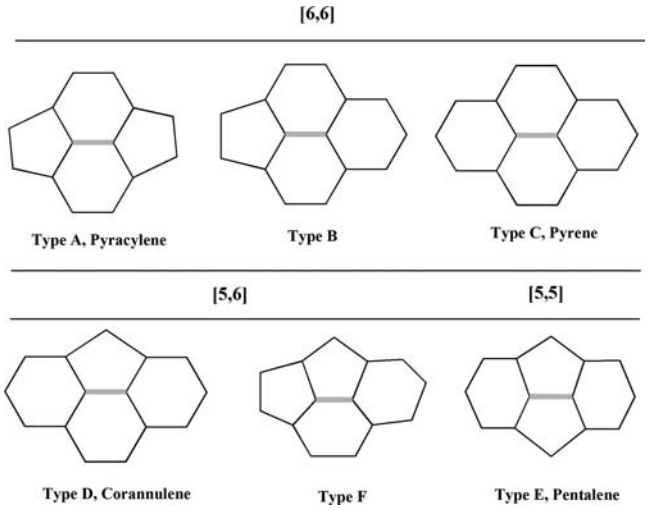

Figure 1. Representations of the different [6,6], [5,6], and [5,5] bond types that may be present in fullerene structures.

Encapsulation also has a major impact on the stability of the different isomers of the cage.[13] It has been shown that the HOMO−LUMO gap of the TNT EMFs, which is related to their chemical stability, can be estimated from the LUMO+3−LUMO+4 gap of the free fullerene, i.e., only those free cages that have large LUMO+3−LUMO+4 gaps produce stable, experimentally observed EMFs.[14] Apparently, however, the size of the cage is also an important factor that determines the stability of the TNT EMFs. Thus, while the encapsulation of Sc_3N is produced in the fullerene cage C_{78}:5 ($D_{3h'}$), larger metal clusters such as Y_3N, La_3N, and Lu_3N are forced to adopt a pyramidal configuration in this cage, which makes the corresponding TNT EMF species 20.0, 37.7, and 14.8 kcal mol^{-1} less stable (at the PBE/TZ2P level of theory) than their counterparts encapsulated inside the non-isolated-pentagon-rule (non-IPR) C_{78} isomer C_2:22010.[13]

Exohedral (exterior) functionalization of EMFs is important for modifying their chemical and physical properties and might be used in a variety of fields ranging from molecular electronics to biomedical applications.[3,15] The first reaction of a TNT EMF to be described was the Diels−Alder cycloaddition on $Sc_3N@I_h$-C_{80}, which was reported in 2002.[16−18] In this case, the reaction took place over a corannulene-type [5,6] bond (type D in Figure 1). Different bond types exist in fullerene structures, and a first classification can be performed by considering on one hand those bonds that are situated between two hexagonal rings (called [6,6] bonds) and on the other hand those located between hexagonal and pentagonal rings ([5,6] bonds) (see Figure 1). In 2005, the 1,3-dipolar cycloaddition was produced on the same $Sc_3N@I_h$-C_{80} TNT EMF,[19] and a similar reaction pattern (i.e., over corannulene-type [5,6] bonds) was found. Interestingly, the same reaction over the yttrium-based TNT EMF $Y_3N@I_h$-C_{80} gives the addition over the [6,6] bond of type B (see Figure 1).[11,19] Experiments with encapsulated mixed-metal clusters (i.e., Sc_2YN and ScY_2N) showed that the transition is smooth. The reaction over $Sc_2YN@I_h$-C_{80} produced only the [5,6] adduct, similar to $Sc_3N@I_h$-C_{80}. A change in regioselectivity occurred for $ScY_2N@I_h$-C_{80}, where the [6,6] regioisomer appeared as minor adduct,[20] and finally, only the [6,6] regioisomer is obtained for $Y_3N@I_h$-C_{80}. Therefore, as discussed in previous studies,[11] the exohedral reactivity of the EMFs seems to be dictated by the nature of the endohedral metal cluster. Let us briefly add here that the Bingel−Hirsch reaction has also been successfully carried out over the same [6,6] bond on $Y_3N@I_h$-C_{80}. In this case, the C−C bond at the site of the addition is broken in the final adduct, as indicated by the X-ray crystal structure, which also showed that one of the yttrium atoms of the metal cluster is positioned near the site of the cleaved bond.[21]

Although the fullerenic cage of the most stable isomer of $Sc_3N@C_{80}$ has icosahedral (I_h) symmetry, the D_{5h} isomer ($Sc_3N@D_{5h}$-C_{80}) has also been synthesized and exohedrally functionalized.[16−18,21,22] Actually, the Diels−Alder and 1,3-dipolar cycloadditions on $Sc_3N@D_{5h}$-C_{80} (and also on $Lu_3N@D_{5h}$-C_{80}) were recently reported.[22] Theoretical studies confirmed the lower stability of the free D_{5h} isomer of C_{80}, which is found to be 21.1 kcal mol^{-1} less stable than the I_h isomer with the PBE/TZ2P method.[23] This energy difference does not hamper the reactivity of the less stable isomer. Instead, the D_{5h} isomer is much more reactive than the I_h isomer, as it contains pyracylene-type [6,6] bonds (type A in Figure 1, absent in the I_h isomer), where the reactions took place. It is worth noting that in some of these reactions, the thermodynamic- and kinetic-control products do not correspond to the same adduct, as observed by Dorn and co-workers[24] in the synthesis of the *N*-tritylpyrrolidinofullerene when starting from $Sc_3N@C_{80}$.[24] In the case of $Y_3N@$(*N*-ethylpyrrolidino-C_{80}), the isomerization from the [6,6] to the [5,6] regioisomer is possible under thermal treatment through a pirouette-type mechanism instead of via retrocycloaddition.[25−27]

More scarce and recent are the examples of exohedral chemistry on EMFs of C_{78}. Last year, Cai et al.[28] synthesized the first *N*-tritylpyrrolidino derivatives of $Sc_3N@D_{3h}$-C_{78} by

(13) Popov, A. A.; Krause, M.; Yang, S.; Wong, J.; Dunsch, L. *J. Phys. Chem. B* **2007**, *111*, 3363–3369.
(14) Campanera, J. M.; Bo, C.; Poblet, J. M. *Angew. Chem., Int. Ed.* **2005**, *44*, 7230–7233.
(15) Pinzón, J. R.; Plonska-Brzezinska, M. E.; Cardona, C. M.; Athans, A. J.; Gayathri, S. S.; Guldi, D. M.; Herranz, M. A.; Martín, N.; Torres, T.; Echegoyen, L. *Angew. Chem., Int. Ed.* **2008**, *47*, 4173–4176.
(16) Iezzi, E. B.; Duchamp, J. C.; Fletcher, K. R.; Glass, T. E.; Dorn, H. C. *Nano Lett.* **2002**, *2*, 1187–1190.
(17) Lee, H. M.; Olmstead, M. M.; Iezzi, E.; Duchamp, J. C.; Dorn, H. C.; Balch, A. L. *J. Am. Chem. Soc.* **2002**, *124*, 3494–3495.
(18) Iezzi, E. B.; Duchamp, J. C.; Harich, K.; Glass, T. E.; Lee, H. M.; Olmstead, M. M.; Bach, A. L.; Dorn, H. C. *J. Am. Chem. Soc.* **2002**, *124*, 524–525.
(19) Cardona, C. M.; Kitaygorodskiy, A.; Ortiz, A.; Herranz, M. A.; Echegoyen, L. *J. Org. Chem.* **2005**, *70*, 5092–5097.
(20) Chen, N.; Fan, L. Z.; Tan, K.; Wu, Y. Q.; Shu, C. Y.; Lu, X.; Wang, C. R. *J. Phys. Chem. C* **2007**, *111*, 11823–11828.
(21) Lukoyanova, O.; Cardona, C. M.; Rivera, J.; Lugo-Morales, L. Z.; Chancellor, C. J.; Olmstead, M. M.; Rodriguez-Fortea, A.; Poblet, J. M.; Balch, A. L.; Echegoyen, L. *J. Am. Chem. Soc.* **2007**, *129*, 10423–10430.
(22) Cai, T.; Xu, L. S.; Anderson, M. R.; Ge, Z. X.; Zuo, T. M.; Wang, X. L.; Olmstead, M. M.; Balch, A. L.; Gibson, H. W.; Dorn, H. C. *J. Am. Chem. Soc.* **2006**, *128*, 8581–8589.
(23) Popov, A. A.; Dunsch, L. *J. Am. Chem. Soc.* **2007**, *129*, 11835–11849.
(24) Cai, T.; Slebodnick, C.; Xu, L.; Harich, K.; Glass, T. E.; Chancellor, C.; Fettinger, J. C.; Olmstead, M. M.; Balch, A. L.; Gibson, H. W.; Dorn, H. C. *J. Am. Chem. Soc.* **2006**, *128*, 6486–6492.
(25) Cardona, C. M.; Elliott, B.; Echegoyen, L. *J. Am. Chem. Soc.* **2006**, *128*, 6480–6485.
(26) Echegoyen, L.; Chancellor, C. J.; Cardona, C. M.; Elliott, B.; Rivera, J.; Olmstead, M. M.; Balch, A. L. *Chem. Commun.* **2006**, 2653–2655.
(27) Rodríguez-Fortea, A.; Campanera, J. M.; Cardona, C. M.; Echegoyen, L.; Poblet, J. M. *Angew. Chem., Int. Ed.* **2006**, *45*, 8176–8180.
(28) Cai, T.; Xu, L.; Gibson, H. W.; Dorn, H. C.; Chancellor, C. J.; Olmstead, M. M.; Balch, A. L. *J. Am. Chem. Soc.* **2007**, *129*, 10795–10800.

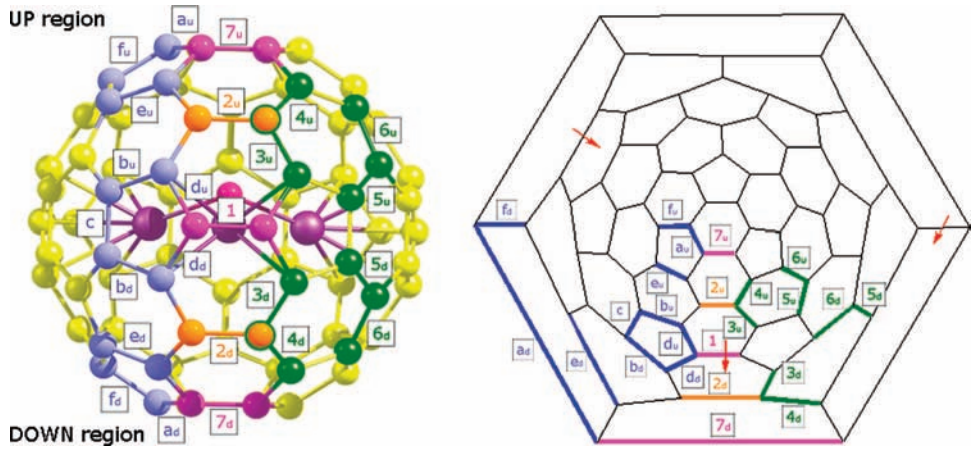

Figure 2. Different nonequivalent bonds of $Y_3N@D_{3h}$-C_{78} are represented. Numbers denote the [6,6] bonds and lowercase letters the [5,6] bonds. The suffix "u" indicates that the considered bond is situated in the *up* region (which is more affected by the nitrogen atom), whereas the suffix "d" denotes the *down* area (which is more influenced by the yttrium atoms). Different colors are used to mark the different bond types: pink, type A; green, type B; orange, type C; blue, type D. The Schlegel diagram, which converts the 3D structure into a 2D representation, is also shown. The positions of the yttrium atoms are marked with red arrows.

means of a 1,3-dipolar cycloaddition. NMR experiments and X-ray crystallographic analysis of the monoadducts showed that the reaction took place over two different type-B [6,6] bonds (bonds **4** and **6** in Figure 2) and not over the pyracylenic [6,6] bonds. More recently, the same group obtained the monoadduct and a dominant symmetric bisadduct through a Bingel−Hirsch cyclopropanation reaction of diethyl bromomalonate and $Sc_3N@D_{3h}$-C_{78}.[29] In this case, the different additions occur at equivalent **6** bonds (type-B [6,6] bonds) of the $Sc_3N@D_{3h}$-C_{78} cage. Interestingly, this reaction does not occur in $Sc_3N@I_h$-C_{80},[11] which is an indication of the higher reactivity of $Sc_3N@D_{3h}$-C_{78} than $Sc_3N@I_h$-C_{80}. Finally, the addition of adamantylidene to $La_2@D_{3h}$-C_{78} and the formation of a bis(silyl) derivative in $Ce_2@D_{3h}$-C_{78} are two additional examples of the reactivity of C_{78}-based EMFs that have just been reported.[30,31]

Recently, we performed a theoretical study of the thermodynamics and kinetics of the Diels−Alder reaction of 1,3-butadiene with either the free fullerene cage D_{3h}-C_{78} or the TNT EMF $Sc_3N@D_{3h}$-C_{78}.[9] The choice of the C_{78} cage was in part motivated by the lack of free rotation of the Sc_3N unit inside the carbon cage. Poblet and co-workers[32] found that the energy barrier for rotation of the Sc_3N moiety was 25.8 kcal mol^{-1} at the BP86/TZP level. This facilitates the theoretical study and allows an evaluation of the change in the reactivity of the bonds depending on the distance to the Sc_3N unit. In our study,[9] we showed that Sc_3N cluster encapsulated inside the C_{78} fullerene cage clearly produces a decrease in its reactivity, and those bonds with scandium atoms facing them become non- or less reactive. Moreover, the introduction of Sc_3N into the D_{3h}-C_{78} cage produces a change in the regioselectivity of the addition, as the reaction over $Sc_3N@D_{3h}$-C_{78} produced the most favorable addition over a type-B [6,6] bond (**6**, see Figure 2), whereas in the case of D_{3h}-C_{78}, the addition was clearly favored on a type-D [5,6] bond (**b**, Figure 2) instead of on the pyracylene bonds (where the reaction occurs in C_{60}).

In this work, our aim was to locate all of the stationary points (minima or saddle points) on the potential energy surface of the Diels−Alder cycloaddition reaction between 1,3-butadiene and each of the nonequivalent bonds of $Y_3N@D_{3h}$-C_{78} and to compare them with those of the recently studied $Sc_3N@D_{3h}$-C_{78} and D_{3h}-C_{78} compounds.[9] The main goal is to discuss the change in reactivity and regioselectivity induced by the change in the encapsulated TNT. As the metal cluster Y_3N is forced to adopt a pyramidal structure inside D_{3h}-C_{78} (see below), two different regions in $Y_3N@D_{3h}$-C_{78} can be differentiated (see Figure 2): the area situated closer to, and therefore more influenced by, the nitrogen atom (the *up* region), and the half-cage farther away from the N atom (the *down* region). In the $Y_3N@D_{3h}$-C_{78} case, 13 nonequivalent [6,6] and 11 nonanalogous [5,6] bonds had to be studied in order to take into account all possible final reaction products (see Figure 2). As a second goal, we are also interested in studying the Diels−Alder reaction for some selected bonds of the C_2-C_{78} isomer, which has been predicted to be the most stable cage for the encapsulation of large TNT clusters such as Y_3N.[13] Therefore, we will also discuss here the thermodynamics of selected bonds in C_2-C_{78}, $Sc_3N@C_2$-C_{78}, and $Y_3N@C_2$-C_{78} in order to investigate the change in the exohedral reactivity of the C_2-C_{78} isomer when different clusters are encapsulated inside.

Computational Details

All of the density functional theory (DFT) calculations were performed with the Amsterdam Density Functional (ADF) program.[33,34] The molecular orbitals (MOs) were expanded in an uncontracted set of Slater-type orbitals (STOs) of double-ζ (DZP) and triple-ζ (TZP) quality containing diffuse functions and one set of polarization functions. In order to reduce the computational time needed to carry out the calculations, the frozen core approximation was used.[34] This approximation is fundamentally different from using effective core potentials (ECPs). Although within the frozen-core

(29) Cai, T.; Xu, L.; Shu, C.; Champion, H. A.; Reid, J. E.; Anklin, C.; Anderson, M. R.; Gibson, H. W.; Dorn, H. C. *J. Am. Chem. Soc.* **2008**, *130*, 2136–2137.
(30) Cao, B.; Nikawa, H.; Nakahodo, T.; Tsuchiya, T.; Maeda, Y.; Akasaka, T.; Sawa, H.; Slanina, Z.; Mizorogi, N.; Nagase, S. *J. Am. Chem. Soc.* **2008**, *130*, 983–989.
(31) Yamada, M.; Wakahara, T.; Tsuchiya, T.; Maeda, Y.; Kako, M.; Akasaka, T.; Yoza, K.; Horn, E.; Mizorogi, N.; Nagase, S. *Chem. Commun.* **2008**, 558–560.
(32) Campanera, J. M; Bo, C.; Olmstead, M. M.; Balch, A. L.; Poblet, J. M. *J. Phys. Chem. A* **2002**, *106*, 12356–12364.
(33) Baerends, E. J.; et al. *ADF*; SCM: Amsterdam, 2006.
(34) te Velde, G.; Bickelhaupt, F. M.; Baerends, E. J.; Fonseca Guerra, C.; van Gisbergen, S. J. A.; Snijders, J. G.; Ziegler, T. *J. Comput. Chem.* **2001**, *22*, 931–967.

approach in ADF, core electrons are not included in the SCF procedure, it *does* include the core orbitals and explicitly orthogonalizes the valence orbitals to them. Moreover, the core density is obtained and included explicitly, albeit with core orbitals that are kept frozen during the SCF procedure. It is therefore preferred over ECPs, which are model Hamiltonians that replace only the *effect* of the core electrons and do not involve core densities or orbitals. Indeed, a recent study by our group on spin-state energies of iron complexes has shown that the results obtained with ECPs are systematically different from those obtained with either STOs or Gaussian-type orbitals (GTOs).[35] Therefore, in this work, core electrons (1s for second period, 1s2s2p for third and fourth period, and 1s2s2p3s3p4s3d for fifth period) were not treated explicitly during the geometry optimizations (frozen core approximation),[34] as this approach was shown to have a negligible effect on the obtained geometries.[36] Scalar relativistic corrections were included self-consistently using the zeroth-order regular approximation (ZORA).[37] A previous study[38] on group 16 hydrides and halogen dimers showed that the effect of the frozen-core approach was small, and the relativistic effects only played a major role for the fifth period onward. Since yttrium is in this period, we investigated here the effect of the frozen core and relativistic effects on bond distances for the isolated TNT clusters. The effect of the frozen core (vs an all-electron basis set) is small, 0.001 Å for Sc_3N and 0.006 Å for Y_3N. Similarly, the inclusion of relativistic effects induces only small changes of 0.002 Å for Sc_3N and 0.008 Å for Y_3N.

An auxiliary set of s, p, d, f, and g STOs was used to fit the molecular density and to represent the Coulomb and exchange potentials accurately for each SCF cycle. Energies and gradients were calculated using the local density approximation (Slater exchange and Vosko−Wilk−Nusair correlation[39]) with nonlocal corrections for exchange (Becke88)[40] and correlation (Perdew86)[41] included self-consistently (i.e., through the use of the BP86 functional). All of the energies reported here were obtained from single-point energy calculations with the TZP basis at geometries that were obtained with the DZP basis (i.e., at the BP86/TZP// BP86/DZP level).

Although it is well-documented that standard DFT functionals like BP86 underestimate energy barriers[42,43] (e.g., in the case of the parent Diels−Alder reaction, BP86/TZP predicts a barrier of 18.6 kcal/mol, i.e., an underestimation of the experimental value by ~6 kcal/mol), this underestimation should be similar for all of the Diels−Alder transition states (TSs) encountered here.[9]

The actual geometry optimizations and TS searches were performed with the QUILD[44] (QUantum-regions Interconnected by Local Descriptions) program, which functions as a wrapper around the ADF program. The QUILD program constructs all of the input files for ADF, runs ADF, and collects all of the data; ADF is used only for the generation of the energy and gradients. Furthermore, the QUILD program uses improved geometry-optimization techniques, such as adapted delocalized coordinates[44] and specially constructed model Hessians with the appropriate number of eigenvalues.[44] The latter is of particular use for TS searches. All of the TSs for the *up* region and all of the TSs for the *down* region that exhibited a difference in the reaction barrier of more than 1 kcal mol^{-1} relative to the *up* region (bonds **e** and **b**) were characterized by computing the analytical[45] vibrational frequencies, in order to have one (*and only one*) imaginary frequency corresponding to the approach of the two reacting carbons (see the Supporting Information).

Pyramidalization angles, introduced by Haddon[46,47] as a measure of the local curvature in polycyclic aromatic hydrocarbons, were calculated using the POAV3 program.[48]

Results and Discussion

The Diels−Alder reaction between 1,3-butadiene and $Y_3N@D_{3h}$-C_{78} was studied in detail for all nonequivalent bonds of the fullerene, and the results are compared to those found for the fullerenes D_{3h}-C_{78} and $Sc_3N@D_{3h}$-C_{78}.[9] As mentioned in the Introduction, the Y_3N unit cannot adopt a planar structure inside the considered D_{3h} isomer, and therefore, two clearly differentiated zones are present. These zones are called the *up* region, which is more influenced by the nitrogen atom close to it, and the *down* region, which is more affected by the yttrium atoms (see Figure 2). We will refer to each different bond according to the nomenclature shown in Figure 2: numbers and lowercase letters refer to [6,6] and [5,6] bonds, respectively, and the subscripts "u" and "d" denote the *up* and *down* regions, respectively. For example, the label $\mathbf{7_u}$ represents the pyracylenic (type-A) [6,6] bond situated in the *up* zone (at the top-center of the left panel in Figure 2), while $\mathbf{a_d}$ refers to the corannulene (type-D) [5,6] bond situated in the *down* zone (near the bottom-center in the same figure).

Reaction Energies for the Diels−Alder Reaction on $Y_3N@D_{3h}$-C_{78}. The reaction energies (ΔE_R) at the BP86/TZP// BP86/DZP level for the *up* and *down* regions are listed in Table 1. As can be seen, differences between the reaction energies of the *up* and *down* regions are always less than 1.6 kcal mol^{-1}. In general, the Diels−Alder reaction is more favored over those bonds situated in the *down* region (especially for bonds $\mathbf{3_d}$, $\mathbf{5_d}$, $\mathbf{d_d}$, and $\mathbf{e_d}$), except for the [6,6] bonds $\mathbf{2_u}$, $\mathbf{4_u}$, and $\mathbf{7_u}$, where the bonds in the *up* region are slightly more reactive. The most stable addition is produced over the [5,6] bond **d**, for which the reaction energies are −13.4 and −15.0 kcal mol^{-1} for $\mathbf{d_u}$ and $\mathbf{d_d}$, respectively. Interestingly, this bond **d** exhibits one of the longest bond distances in the reactant fullerene (1.468 and 1.464 Å for the *up* and *down* regions, respectively, which are exceeded only by the lengths of the [6,6] bonds $\mathbf{2_u}$ and $\mathbf{2_d}$; see Table 2). Short bond distances together with high pyramidalization angles[46−48] have been the most widely used reactivity descriptors to predict the exohedral reactivities of fullerene derivatives.[49] Thus, bonds with rather long C−C bond distances have always been considered to be non- or much less reactive, which is indeed the case for bond **2** (see Table 1). However, our results show that the addition to long C−C bonds is also possible, and even preferred, for highly strained systems such as $Y_3N@D_{3h}$-C_{78}. As far as we know, this is the first case of a cycloaddition reaction where the most stable addition results from the attack on a bond with one of the longest C−C bond distances.

(35) Güell, M.; Luis, J. M.; Solà, M.; Swart, M. *J. Phys. Chem. A* **2008**, *112*, 6384–6391.
(36) Swart, M.; Snijders, J. G. *Theor. Chem. Acc.* **2003**, *110*, 34–41.
(37) van Lenthe, E.; Baerends, E. J.; Snijders, J. G. *J. Chem. Phys.* **1993**, *99*, 4597–4610.
(38) Swart, M.; Bickelhaupt, F. M. *J. Comput. Chem.* **2008**, *29*, 724–734.
(39) Vosko, S. H.; Wilk, L.; Nusair, M. *Can. J. Phys* **1980**, *58*, 1200–1211.
(40) Becke, A. D. *Phys. Rev. A* **1988**, *38*, 3098–3100.
(41) Perdew, J. P. *Phys. Rev. B* **1986**, *33*, 8800–8802.
(42) Goumans, T. P. M.; Ehlers, A. W.; Lammertsma, K.; Würthwein, E.-U.; Grimme, S. *Chem.−Eur. J.* **2004**, *10*, 6468–6475.
(43) Swart, M.; Solà, M.; Bickelhaupt, F. M. *J. Comput. Chem.* **2007**, *28*, 1551–1560.
(44) Swart, M.; Bickelhaupt, F. M. *Int. J. Quantum Chem.* **2006**, *106*, 2536–2544.
(45) Wolff, S. K. *Int. J. Quantum Chem.* **2005**, *104*, 645–659.
(46) Haddon, R. C. *J. Phys. Chem. A* **2001**, *105*, 4164–4165.
(47) Haddon, R. C.; Chow, S. Y. *J. Am. Chem. Soc.* **1998**, *120*, 10494–10496.
(48) Haddon, R. C. *QCPE Bull.* **1988**, *8*, 48; Program QCPE 508/QCMP 044.
(49) Solà, M.; Mestres, J.; Duran, M. *J. Phys. Chem.* **1995**, *99*, 10752–10758.

Table 1. Reaction Energies (ΔE_R, kcal mol^{-1}) and Bond Lengths (Å) in the Final Products of the C−C Bonds over Which the Reaction Took Place (R_{full}) and the Two Newly Formed C−C Bonds (R_{CC})[a]

		$Y_3N@D_{3h}$-C_{78} *up*				$Y_3N@D_{3h}$-C_{78} *down*			
product	bond type	ΔE_R	R_{full}	R_{CC}		ΔE_R	R_{full}	R_{CC}	
1	A [6,6]	−5.4	1.646	1.565	1.565	−5.4	1.646	1.565	1.565
2	C [6,6]	+5.8	1.693	1.577	1.577	+6.6	1.699	1.578	1.578
3	B [6,6]	+0.6	1.727	1.558	1.559	−0.9	1.715	1.561	1.560
4	B [6,6]	−8.7	1.648	1.576	1.563	−7.8	1.650	1.574	1.566
5	B [6,6]	+10.0	1.633	1.576	1.580	+8.7	1.629	1.573	1.579
6	B [6,6]	**−10.6**	1.583	1.570	1.573	**−11.0**	1.581	1.570	1.572
7	A [6,6]	−6.6	1.583	1.574	1.574	−6.1	1.582	1.575	1.575
a	D [5,6]	−3.4	1.629	1.564	1.564	−4.1	1.632	1.563	1.563
b	D [5,6]	−1.7	1.656	1.565	1.568	−1.9	1.661	1.568	1.568
c	D [5,6]	−6.1	1.614	1.563	1.564	−6.1	1.614	1.563	1.564
d	D [5,6]	**−13.4**	1.686	1.556	1.557	**−15.0**	1.678	1.555	1.558
e	D [5,6]	−2.7	1.642	1.563	1.568	−4.1	1.643	1.560	1.563
f	D [5,6]	−5.6	1.612	1.562	1.562	−6.6	1.613	1.562	1.563

[a] Bold values indicate the bonds that are the most reactive under thermodynamic control.

Table 2. Bond Lengths (R_{full}, Å) and Pyramidalization Angles (θ_p, deg) for the Different Bonds in Free and Endohedral Fullerenes

	D_{3h}-C_{78}[a]		$Sc_3N@D_{3h}$-C_{78}[a]		$Y_3N@D_{3h}$-C_{78} *up*		$Y_3N@D_{3h}$-C_{78} *down*	
product	R_{full}	θ_p[b]	R_{full}	θ_p[b]	R_{full}	θ_p[b]	R_{full}	θ_p[b]
1	1.369	10.46	1.440	13.80	1.463	14.03	1.463	14.03
2	1.465	8.58	1.466	8.33	1.475	8.46	1.474	8.55
3	1.432	9.62	1.450	9.26	1.460	9.83	1.448	9.64
4	1.415	9.60	1.426	9.44	1.432	9.22	1.435	9.34
5	1.418	9.53	1.432	8.97	1.443	8.56	1.443	8.67
6	1.420	9.44	1.400	9.99	1.396	9.66	1.398	9.78
7	1.388	11.64	1.400	11.21	1.398	11.17	1.401	11.06
a	1.438	11.64	1.437	11.21	1.439	11.17	1.440	11.06
b	1.410	10.49	1.446	9.73	1.455	10.10	1.457	9.89
c	1.465	10.32	1.423	9.27	1.423	9.02	1.423	9.02
d	1.446	10.56	1.452	12.00	1.468	12.62	1.464	12.38
e	1.438	10.38	1.449	10.92	1.454	10.60	1.453	10.70
f	1.442	11.13	1.432	10.88	1.431	10.58	1.431	10.59

[a] Values from ref 9. [b] Reported pyramidalization angles represent the average over the two atoms that constitute the bond under consideration.

The introduction of metal clusters such as Sc_3N or Y_3N inside the C_{78} fullerene cage leads to an increase in the volume of C_{78}[32] and thus to a more deformed system (the volume as measured by the GEPOL93[50] procedure is increased by 40.3 and 88.6 bohr^3 for $Sc_3N@D_{3h}$-C_{78} and $Y_3N@D_{3h}$-C_{78}, respectively, relative to free C_{78}; see Figure 3). Moreover, the most important deformation is produced when the large Y_3N cluster is introduced; the deformation energy of the C_{78} cage for encapsulating Sc_3N is 32.2 kcal mol^{-1} while that for Y_3N is significantly higher (67.5 kcal mol^{-1}) at the BP86/TZP//BP86/DZP level of theory. As can be seen in Figure 3, the most deformed regions are the pyracylene rings situated closer to the yttrium atoms. The type-A, -B, and -C [6,6] bonds **1**, **2**, and **3**, respectively, and the [5,6] bond **d** are situated in this more influenced and deformed area (see Figure 2). Therefore, an important increase of these bond distances relative to those in the free fullerene or the scandium-based endohedral compound is produced (see Table 2). Larger pyramidalization angles are also found for bonds **1** (14.0°) and **d** (12.6° and 12.4° for $\mathbf{d_u}$ and $\mathbf{d_d}$, respectively). As previously mentioned, the [5,6] bond **d** is thermodynamically the most reactive. The rest of the [6,6] bonds situated in this deformed zone present reaction energies ranging from endothermic (+5.8, +6.6, and +0.6 kcal mol^{-1} for $\mathbf{2_u}$, $\mathbf{2_d}$, and $\mathbf{3_u}$, respectively) to slightly exothermic (−0.9 and −5.4 kcal mol^{-1} for $\mathbf{3_d}$ and **1**, respectively) (Table 1).

The second most thermodynamically favorable regioisomer is obtained when the reaction takes place over the [6,6] bonds

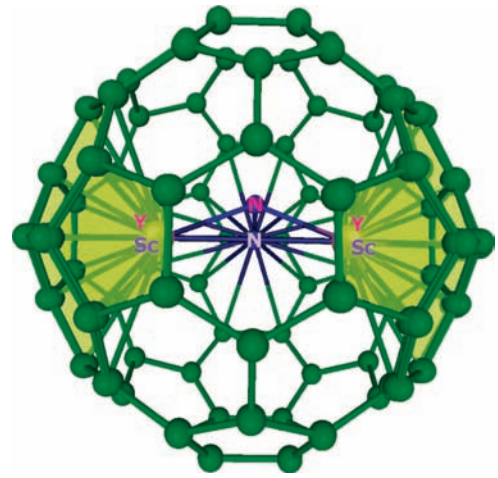

Figure 3. Superposition of the $Y_3N@D_{3h}$-C_{78} and $Sc_3N@D_{3h}$-C_{78} structures. The main differences are localized on the pyramidalization of the nitrogen of the cluster (h = 0.693 Å) and the pyracylene units situated close to the metal atoms (colored in light green).

$\mathbf{6_u}$ and $\mathbf{6_d}$ (−10.6 and −11.0 kcal mol^{-1}, respectively). These [6,6] bonds have the smallest C−C bond distances (1.396 and 1.398 Å), together with the [6,6] bonds **7** and **4** (∼1.400 and ∼1.433 Å, respectively). The reactions over the type-B [6,6] bonds $\mathbf{4_u}$, $\mathbf{4_d}$, $\mathbf{7_u}$, and $\mathbf{7_d}$ also give exothermic reaction energy values of −8.7, −7.8, −6.6, and −6.1 kcal mol^{-1}, respectively. Therefore, the Diels−Alder reaction over [6,6] bonds in these systems is usually favored for bonds with short C−C bond

(50) Pascual-Ahuir, J. L.; Silla, E.; Tuñón, I. *J. Comput. Chem.* **1994**, *15*, 1127–1138.

Table 3. Reaction Barriers ($\Delta E^{\ddagger}$, kcal mol^{-1}) and Bond Lengths (R_{CC}, Å) for the Bonds Being Formed at the TS[a]

		$Y_3N@D_{3h}$-C_{78} *up*			$Y_3N@D_{3h}$-C_{78} *down*		
product	bond type	$\Delta E^{\ddagger}$	R_{CC}		$\Delta E^{\ddagger}$	R_{CC}	
1	A [6,6]	20.1	1.754	2.622	20.1	1.754	2.622
2	C [6,6]	26.2	1.707	2.509	27.0	1.702	3.532
3	B [6,6]	26.6	1.712	2.470	27.1	1.758	2.512
4	B [6,6]	20.6	1.987	2.503	21.1	1.911	2.663
5	B [6,6]	29.8	1.728	2.419	30.2	1.739	2.455
6	B [6,6]	**19.2**	1.980	2.571	**18.3**	1.882	2.889
7	A [6,6]	20.8	2.108	2.276	20.6	2.010	2.403
a	D [5,6]	22.9	1.767	2.715	23.0	1.752	2.748
b	D [5,6]	21.4	1.681	2.603	23.1	1.757	2.681
c	D [5,6]	22.5	1.827	2.756	22.5	1.827	2.756
d	D [5,6]	**17.6**	1.875	2.737	**17.1**	1.915	2.677
e	D [5,6]	23.3	1.701	2.653	**17.2**	1.856	3.284
f	D [5,6]	22.7	1.787	2.707	21.9	1.787	2.707

[a] Bold values indicate the bonds that are the most reactive under kinetic control.

distances and large pyramidalization angles, while [5,6] bonds are more reactive either when they have long bond distances with large pyramidalization angles (bond **d**, the most favorable addition site among all of the bonds considered) or short bond distances with moderate pyramidalization angles (**c** and **f**, with bond distances of 1.423 and 1.431 Å and pyramidalization angles of 9.02 and 10.6°, respectively). The reaction energies found for these more reactive [5,6] bonds **c**, $\mathbf{f_u}$, and $\mathbf{f_d}$ are −6.1, −5.6, and −6.6 kcal mol^{-1}, respectively. The [5,6] bonds that present intermediate bond distances (from 1.440 to 1.450 Å) present slightly exothermic reaction energies (from −1.7 to −4.1 kcal mol^{-1}).

Energy Barriers for the Diels−Alder Reaction on $Y_3N@D_{3h}$-C_{78}. The energy barriers of the reaction for all of the nonequivalent bonds in the *up* and *down* regions were also determined (Table 3). In all cases, the TS search started from a symmetric structure, and the optimization procedure led to a concerted but asynchronic TS.[51] Differences between *up* and *down* energy barriers are always less than 1.7 kcal mol^{-1}, except for bond **e**, in which the $\mathbf{e_d}$ energy barrier is 4.1 kcal mol^{-1} lower than that for $\mathbf{e_u}$. Interestingly, the attack on the long C−C bond **d** is also the kinetically most favorable among all of the bonds considered (with energy barriers of 17.6 and 17.1 kcal mol^{-1} for $\mathbf{d_u}$ and $\mathbf{d_d}$, respectively). Therefore, the cycloaddition reaction over this long and highly pyramidalized bond is favored not only from the thermodynamic point of view but also from the kinetic one. Of course, the larger the pyramidalization angle, the less the system has to be deformed for the reaction to proceed, which facilitates the reaction. The reason for the high reactivity of this long bond, apart from the large pyramidalization angle, will be discussed in the next section.

The second most stable products $\mathbf{6_u}$ and $\mathbf{6_d}$ (with reaction energies of −10.5 and −11.0 kcal mol^{-1}) also present low reaction barriers of 19.2 and 18.3 kcal mol^{-1} respectively, whereas bond $\mathbf{e_d}$, with a reaction energy of only −4.1 kcal mol^{-1}, presents the second most favorable activation barrier (17.2 kcal mol^{-1}). Moreover, a remarkable difference between the reaction barriers for bond **e** in the *up* and *down* regions is found (23.3 and 17.2 kcal mol^{-1} for $\mathbf{e_u}$ and $\mathbf{e_d}$, respectively). This difference in energy barrier cannot be attributed to a shorter C−C bond length or a larger pyramidalization angle in $\mathbf{e_d}$, because these properties are approximately the same for $\mathbf{e_u}$ and $\mathbf{e_d}$. An analysis of the molecular orbitals (MOs) shows that the N lone-pair electrons interact more effectively with the closer $\mathbf{e_u}$ bond than with the $\mathbf{e_d}$ bond (see occupied MOs 37 and 38 in Figure 4). The participation of the $\mathbf{e_u}$ bond in the occupied N lone-pair orbital pushes the lowest-lying unoccupied MOs (LUMOs) having contributions from the $\mathbf{e_u}$ bond to higher energies, and as a result, there is a deactivation of this bond. In LUMO+7 (2), only bond $\mathbf{e_d}$ presents orbitals suitable for interacting with the HOMO of the diene, whereas in LUMO+9,

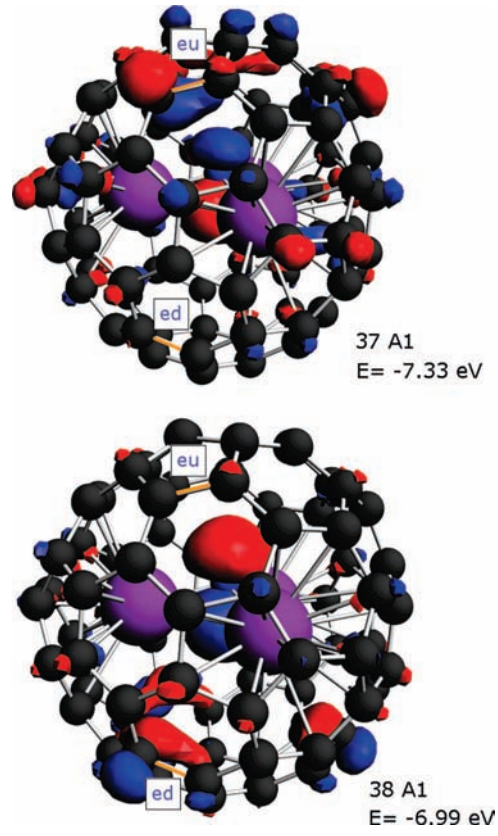

Figure 4. Representations of the (top) HOMO-9 (37 A1) and (bottom) HOMO-8 (38 A1) occupied molecular orbitals of $Y_3N@D_{3h}$-C_{78}, showing that the N lone-pair electrons interact more effectively with the closer $\mathbf{e_u}$ bond than with the $\mathbf{e_d}$ bond (isosurface value 0.03 a.u).

(51) Bachrach, S. M.; White, P. B. *THEOCHEM* **2007**, *819*, 72–78.

(52) We are aware that the virtual orbitals are not strictly optimized during the SCF process and that their physical meaning is therefore questionable. However, we consider that the present argument, i.e., that the $\mathbf{e_u}$ bond is less activated because of its interaction with the N atom of the pyramidalized Y_3N unit, holds irrespective of the shape and energetic ordering of the virtual orbitals.

Table 4. Reaction Energies ΔE_R and Reaction Barriers $\Delta E^{\ddagger}$ for the Free Cage and the Endohedral Derivatives[a]

		ΔE_R (kcal mol^{-1})			$\Delta E^{\ddagger}$ (kcal mol^{-1})		
product	bond-type	D_{3h}-C_{78}[b]	$Sc_3N@D_{3h}$-C_{78}[b]	$Y_3N@D_{3h}$-C_{78}[c]	D_{3h}-C_{78}[b]	$Sc_3N@D_{3h}$-C_{78}[b]	$Y_3N@D_{3h}$-C_{78}[c]
1	A [6,6]	**−16.0**	4.0	−5.4	**12.2**	23.8	**20.1**
2	C [6,6]	12.5	6.1	6.6	30.2	27.1	27.0
3	B [6,6]	1.8	9.2	−0.9	21.7	28.9	27.1
4	B [6,6]	−9.2	**−9.7**	−7.8	14.8	**20.0**	21.1
5	B [6,6]	0.9	5.9	8.7	14.4	27.6	30.2
6	B [6,6]	4.0	**−12.7**	−11.0	17.2	18.5	18.3
7	A [6,6]	**−18.8**	−7.6	−6.1	**13.5**	20.1	20.6
a	D [5,6]	−8.8	−6.0	−4.1	17.2	21.5	23.0
b	D [5,6]	**−23.9**	−4.3	−1.9	**12.5**	20.7	23.1
c	D [5,6]	−13.3	**−10.4**	−6.1	16.7	**20.1**	22.5
d	D [5,6]	−5.2	−7.6	**−15.0**	22.1	19.7	**17.1**
e	D [5,6]	−13.8	−4.9	−4.1	15.3	22.3	**17.1**
f	D [5,6]	−5.9	−6.5	−6.6	18.0	21.5	21.9

[a] Bold values indicate the bonds that are the most reactive. [b] Values from ref 9. [c] Only the results for the *down* region are reported here.

the two bonds $\mathbf{e_u}$ and $\mathbf{e_d}$ can interact equally (see LUMO+7 (2) and LUMO+9 in Figure S1 of the Supporting Information).[52] In addition, it should be noted that addition over bond $\mathbf{e_u}$ breaks a bonding interaction between the N atom and this $\mathbf{e_u}$ bond (see Figure 4), which disfavors this attack, while for bond $\mathbf{e_d}$, the N−$\mathbf{e_d}$ interaction is antibonding, thus favoring the cycloaddition. Consequently, the reaction over bond $\mathbf{e_d}$ is more favorable both kinetically and thermodynamically, as $\mathbf{e_d}$ presents orbitals suitable for interaction at lower energy and also because the reaction breaks an antibonding interaction between the $\mathbf{e_d}$ bond and the nitrogen atom. Interactions of the N lone-pair orbital with orbitals located in bonds different from **e** are insignificant.

The pyracylenic (or type-A) [6,6] bonds **1** and **7** present relatively low reaction barriers of ∼20 kcal mol^{-1}. The activation barrier obtained for the type-B [6,6] bond **4** is also of the same magnitude. The rest of the [6,6] bonds (**2**, **3**, and **5**) exhibit not only the most endothermic reaction energies but also the highest activation barriers (from 26.2 kcal mol^{-1} for $\mathbf{2_u}$ to 30.2 kcal mol^{-1} for $\mathbf{5_d}$). The rest of the type-D [5,6] bonds present moderate reaction barriers ranging from 21.4 kcal mol^{-1} for $\mathbf{a_u}$ to 23.30 kcal mol^{-1} for $\mathbf{e_u}$.

In general, one finds that reactions with larger exothermicities also have lower energy barriers (e.g., the attacks at bonds **d** and **6**), while those with larger endothermicities have higher barriers (e.g., the attacks at bonds **2** and **5**). However, the connection between the thermodynamic and kinetic results does not always apply:[9,24] for example, reaction over bond **e** has a low energy barrier, corresponding to a very reactive bond, but it is only slightly exothermic.

Effect of the Cluster Nature and Fullerene Strain on the Exohedral Reactivity of the D_{3h} Isomer of C_{78}. We previously studied the Diels–Alder reaction over all of the nonequivalent bonds of the free fullerene cage D_{3h}-C_{78} and its scandium-based endohedral derivative $Sc_3N@D_{3h}$-C_{78}.[9] Therefore, a direct comparison with the present results for $Y_3N@D_{3h}$-C_{78} can easily be made. The same isomer (D_{3h}) is used in the three different cases, so any differences in reactivity can be directly attributed to the nature of the cluster atom encapsulated inside the cage and the strain energy of the fullerene cage studied.

The Diels–Alder reaction energies as well as the activation barriers for $Y_3N@D_{3h}$-C_{78}, $Sc_3N@D_{3h}$-C_{78}, and D_{3h}-C_{78} are reported in Table 4 and represented in Figures 5 and 6. The D_{3h}-C_{78} fullerene contains the pyracylene-type [6,6] bonds that are highly reactive in C_{60}; however, the reaction on the free fullerene over the [5,6] bond **b** is clearly favored from both the thermodynamic and kinetic points of view.[9] The pyracylenic

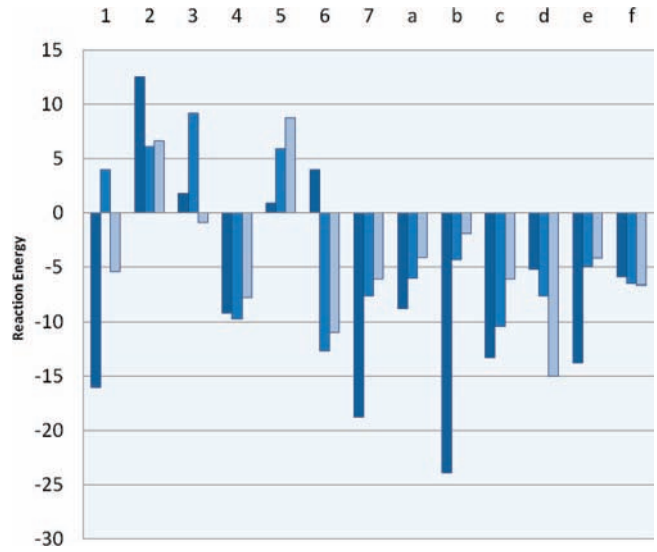

Figure 5. Comparison of the reaction energies (in kcal mol^{-1}) found for the Diels–Alder reaction over the nonequivalent bonds of the free D_{3h}-C_{78} cage (dark blue), $Sc_3N@D_{3h}$-C_{78} (blue), and $Y_3N@D_{3h}$-C_{78} (light blue). For the last of these, energies are included only for bonds in the *down* region.

bonds **7** and **1** present the second and the third most favorable reaction energies. When the Sc_3N cluster is encapsulated inside the cage, the reaction in general becomes less exothermic and/or the reaction barriers increase, with some exceptions (**2**, **4**, **6**, **d**, and **f**). Encapsulation of the Sc_3N unit in D_{3h}-C_{78} decreases the reactivity of the cage because charge transfer from the TNT to C_{78} leads to LUMOs with higher energies, which make them less suitable for the interaction with the diene.[9] In $Sc_3N@D_{3h}$-C_{78}, the Diels–Alder cycloaddition over the type-B [6,6] bond **6**, which presents a short C–C bond distance and is situated far away from the scandium atoms, is clearly favored. The other favorable additions are those over the type-B [6,6] bond **4** and the type-D [5,6] bond **c**. This concurs with work by Cai and co-workers,[28] who synthesized the *N*-tritylpyrrolidino derivatives of $Sc_3N@D_{3h}$-C_{78}, where the reaction takes places over the type-B [6,6] bonds **4** and **6**.

As we have seen, there is a clear general reduction in exohedral reactivity in going from D_{3h}-C_{78} to $Sc_3N@D_{3h}$-C_{78}. In turn, the reactivity of most of the bonds decreases slightly in going from $Sc_3N@D_{3h}$-C_{78} to $Y_3N@D_{3h}$-C_{78}. This reactivity reduction is due to the slightly larger electron transfer from the Y_3N unit to the fullerene, which pushes the LUMOs further

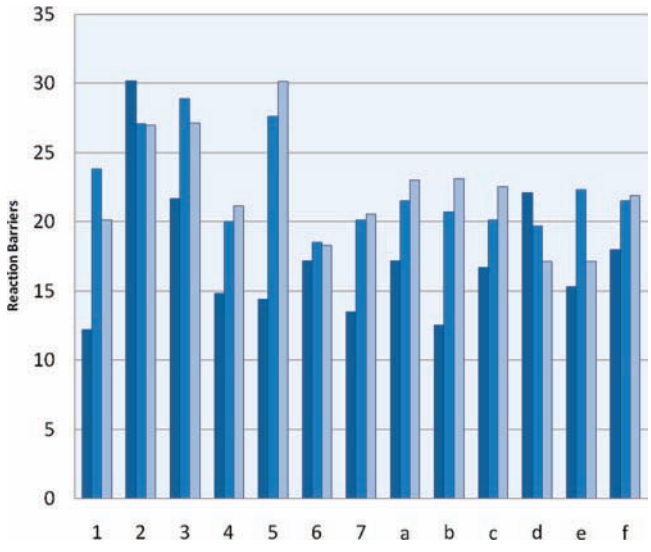

Figure 6. Comparison of the reaction barriers (in kcal mol^{-1}) found for the Diels−Alder reaction over the nonequivalent bonds of the free D_{3h}-C_{78} cage (dark blue), $Sc_3N@D_{3h}$-C_{78} (blue), and $Y_3N@D_{3h}$-C_{78} (light blue). For the last of these, barriers are included only for bonds in the *down* region.

up, leading to a larger HOMO−LUMO gap in $Y_3N@D_{3h}$-C_{78} than in $Sc_3N@D_{3h}$-C_{78} (1.26 and 1.22 eV, respectively). However, the Diels−Alder reactions over bonds **1**, **3**, and **d**, which are situated near the yttrium atoms, are enhanced both thermodynamically and kinetically, leading to the most favorable addition for the case of bond **d**.

The exohedral derivatization of the scandium-based endohedral compound is basically preferred when the reaction occurs over short type-B [6,6] bonds situated far away from the scandium influence. However, in the case of $Y_3N@D_{3h}$-C_{78}, those bonds situated close to the yttrium atoms show enhanced reactivity, and the reaction over the longest and highly pyramidalized [5,6] bond **d** becomes clearly favored. This change in the reactivity might be attributed to the nature of the cluster but also to the strain suffered by the fullerene cage because of the encapsulated TNT unit. A theoretical study showed that the most stable C_{78} isomer for the encapsulation of the Y_3N cluster is the non-IPR C_2:22010. The $Y_3N@C_2$-C_{78} TNT EMF is 20.2 kcal mol^{-1} more stable (at the BP86/TZP//BP86/DZP level) than the $Y_3N@D_{3h}$-C_{78} TNT EMF considered here.[13,23] It should be noted that this energy difference in principle does not hinder the reactivity and/or stability of the less stable isomer, as was shown for the I_h and D_{5h} isomers of C_{80}, both of which have been observed experimentally and reported to be reactive. In particular, the free D_{5h} isomer of C_{80} is the least stable by 21.1 kcal mol^{-1} (at the PBE/TZ2P level), and its endohedral derivative is the most reactive.[22] Thus, in comparison with $Sc_3N@D_{3h}$-C_{78}, the encapsulation of the Y_3N cluster inside the D_{3h} cage leads to a more deformed cage, with highly pyramidalized atoms and larger bond distances in the area situated close to the metal atoms (see Figure 3). The reaction over all of the bonds situated in this region is enhanced relative to $Sc_3N@D_{3h}$-C_{78}, as during the cycloaddition process, the high fullerene strain in this zone is reduced and the pyramidalization of the attacked carbon atoms increases, giving the Y_3N unit the extra space it needs to adopt a less pyramidalized configuration (see Table S1 in the Supporting Information). Recently, Chaur et al.[53] investigated experimentally the Bingel reaction over the gadolinium-based endohedral fullerenes $Gd_3N@C_{80}$ and $Gd_3N@C_{84}$. Interestingly, the reactivity of the smaller C_{80} cage is clearly enhanced relative to the larger C_{84} derivative. This observation is in concordance with our theoretical results, as the introduction of large metal clusters inside relatively small cages produces a large amount of strain that makes the compound more reactive.

The space gained after cycloaddition would be even larger if the reaction broke the **1**, **3**, and **d** bonds, leading to open adducts (i.e., open fulleroid structures). This is indeed what happens if singlet methylene instead of 1,3-butadiene attacks these three bonds to yield $Y_3N@D_{3h}$-C_{78}−CH_2 (reaction energies are given in Table S2 in the Supporting Information). An analogous situation has been discussed experimentally and through DFT calculations by Echegoyen and co-workers[21] when analyzing the cycloaddition of bromomalonates to $Y_3N@C_{80}$. According to these authors, this reaction always leads to open fulleroid derivatives with high stability. They concluded that the interaction of the metal with the carbon cage and the deformation of the cage induced by the TNT favor the fulleroid structure.[21] In the case of the Diels−Alder reaction,[54] the more rigid structure of the diene does not allow for a complete opening of the attacked bond, and the final C−C distances are shorter (1.646, 1.727, and 1.686 Å for **1**, **3**, and **d**, respectively; see Table 1) than they would be in open adducts (∼2.2 Å). Finally, the deformation energies at the TS for the diene fragment, which are calculated as the difference between the energy of the diene in the geometry it has in the TS and that of the optimized free diene, are significantly higher in the case of the attacks on bonds **1** and **3** than for attack on bond **d** (∼20 and ∼24 kcal mol^{-1} for **1** and **3**, respectively, compared with 14 kcal mol^{-1} for bond **d**; see Table S3 in the Supporting Information), while the deformation energies of the C_{78} fragment remain similar. Therefore, it seems that the Diels−Alder addition over bond **d** is preferred because, for a similar C−C bond lengthening in the C_{78} cage, the C−C bond length in the TS of the addition to **d** is more appropriate for the attack of the diene that is not forced to undergo a large deformation. This makes the addition over bond **d** much more favorable.

The results obtained in our work are in line with a previous study[21] showing that the Bingel−Hirsch $Y_3N@C_{80}$−$C(CO_2CH_2Ph)_2$ adduct has an open [6,6] bond at the site of addition, with one of the yttrium atoms facing the addition site, while in the 1,3-dipolar cycloaddition adduct $Y_3N@C_{80}$−$(CH_2)_2NEt$, the Y_3N group is oriented so that there is a metal atom on each side of the attacked [5,6] site.

The Diels−Alder Reaction on Some Selected Bonds of $Y_3N@C_2$-C_{78}. A recent theoretical study[13] has shown that the D_{3h} isomer is not the most suitable cage for encapsulating the Y_3N cluster; rather, the C_2 isomer is the most suitable one, and experimental spectroscopic studies of the recently isolated TNT EMF $Tm_3N@C_{78}$[55] and the major isomer of $Dy_3N@C_{78}$[13] have shown that their carbon cages (of C_2 symmetry) are different from that of $Sc_3N@C_{78}$ (of D_{3h} symmetry). The structure and

(53) Chaur, M. N.; Melin, F.; Athans, A. J.; Elliott, B.; Walker, K.; Holloway, B. C.; Echegoyen, L. *Chem. Commun.* **2008**, 2665–2667.
(54) Cases, M.; Duran, M.; Mestres, J.; Martin, N.; Solà, M. In *Fullerenes for the New Millennium*; Kamat, P. V., Guldi, D. M., Kadish, K. M., Eds.; The Electrochemical Society: Pennington, NJ, 2001; Vol. 11, p 244−269.
(55) Krause, M.; Wong, J.; Dunsch, L. *Chem.−Eur. J.* **2005**, *11*, 706–711.

Table 5. Bond Distances (R_{full}, Å) and Pyramidalization Angles (θ_p, deg) for the Different Bond Types in Free C_2-C_{78} and Its Endohedral Derivatives

		C_2-C_{78}		$Sc_3N@C_2$-C_{78}		$Y_3N@C_2$-C_{78}	
product	bond type	R_{full}	θ_p[a]	R_{full}	θ_p[a]	R_{full}	θ_p[a]
***C*$_2$-E**	[5,5]	1.442	15.73	1.431	16.26	1.436	16.07
***C*$_2$-A**	[6,6]	1.387	11.87	1.405	11.48	1.418	12.01
***C*$_2$-B1**	[6,6]	1.423	9.61	1.416	9.66	1.414	9.47
***C*$_2$-B2**	[6,6]	1.408	8.96	1.415	9.01	1.416	8.93
***C*$_2$-B3**	[6,6]	1.441	11.03	1.433	10.53	1.455	11.37
***C*$_2$-F**	[5,6]	1.396	13.67	1.430	13.83	1.431	13.52
***C*$_2$-Dl**	[5,6]	1.444	10.64	1.455	11.21	1.477	12.20
***C*$_2$-Ds**	[5,6]	1.434	9.81	1.418	9.86	1.419	9.75

[a] Reported pyramidalization angles represent the average over the two atoms that constitute the bond under consideration.

Table 6. Reaction Energies (ΔE_R, kcal mol^{-1}) and Bond Lengths (Å) in the Final Products of the C−C Bonds over Which the Reaction Took Place (R_{full}) and the Two Newly Formed C−C Bonds (R_{CC})[a]

		C_2-C_{78}				$Sc_3N@C_2$-C_{78}				$Y_3N@C_2$-C_{78}			
product	bond type	ΔE_R	R_{full}	R_{CC}		ΔE_R	R_{full}	R_{CC}		ΔE_R	R_{full}	R_{CC}	
***C*$_2$-E**	[5,5]	**−42.6**	1.569	1.550	1.552	**−28.9**	1.593	1.541	1.544	**−25.9**	1.608	1.547	1.548
***C*$_2$-A**	[6,6]	−21.6	1.563	1.565	1.580	−6.3	1.579	1.561	1.580	−2.6	1.604	1.565	1.579
***C*$_2$-B1**	[6,6]	−7.8	1.592	1.574	1.592	−0.7	1.600	1.575	1.579	+2.2	1.599	1.575	1.580
***C*$_2$-B2**	[6,6]	−10.2	1.583	1.581	1.583	+0.5	1.595	1.569	1.581	+1.8	1.599	1.569	1.581
***C*$_2$-B3**	[6,6]	−7.2	1.616	1.573	1.580	−0.8	1.625	1.569	1.571	−3.5	1.684	1.567	1.570
***C*$_2$-F**	[5,6]	**−32.4**	1.566	1.553	1.567	**−9.0**	1.598	1.556	1.561	**−8.4**	1.604	1.558	1.561
***C*$_2$-Dl**	[5,6]	**−25.1**	1.603	1.569	1.570	−3.7	1.659	1.561	1.561	**−10.3**	1.701	1.556	1.556
***C*$_2$-Ds**	[5,6]	−15.1	1.580	1.569	1.575	**−6.5**	1.593	1.561	1.568	−4.4	1.595	1.561	1.567

[a] Bold values indicate the bonds that are the most reactive.

spectroscopic properties of $Y_3N@C_{78}$, $Tm_3N@C_{78}$, and $Dy_3N@C_{78}$ are assumed to be similar because of the similarity of the ionic radii of their metal atoms: 0.90 Å for Y, 0.91 Å for Dy, and 0.87 Å for Tm.[56] For this reason, we will briefly discuss the same Diels−Alder cycloaddition in free and TNT-encapsulated C_2-C_{78} to get a quick insight into regioselectivity changes induced by encapsulation in this fullerenic cage. The analysis is carried out using only reaction energies, as we have seen that in most cases, the kinetic and thermodynamic trends are similar.

On the basis of the previous reactivity patterns mentioned for the D_{3h} cage, and because of the large number of nonequivalent bonds in the non-IPR C_2 isomer (more than 60 different bonds), we investigated the Diels−Alder reaction over some selected bonds that satisfy the reactivity trends found for the D_{3h} isomer. In this way, we selected eight different bonds of $Y_3N@C_2$-C_{78} (see Tables 5 and 6). First, we examined two bonds that are present only in non-IPR structures: one type-E [5,5] bond, labeled ***C*$_2$-E** (1.436 Å, 16.07°), and one type-F [5,6] bond, denoted as ***C*$_2$-F** (1.431 Å, 13.52°). Second, we studied two different type-B [6,6] bonds that exhibit short bond distances (∼1.415 Å) and are situated far away from the cluster influence, with pyramidalization angles of 9.47 and 8.93° (***C*$_2$-B1** and ***C*$_2$-B2**, respectively), as well as another type-B [6,6] bond close to the yttrium atoms (***C*$_2$-B3**) with a large bond length and pyramidalization angle (1.455 Å, 11.37°). Third, we investigated the cycloaddition reaction over two different type-D [5,6] bonds, one (***C*$_2$-Dl**) that has an extremely large C−C bond distance (1.477 Å) and is highly pyramidalized (12.20°) and situated close to one of the yttrium atoms, and another (***C*$_2$-Ds**) that has a short bond distance (1.419 Å, 9.75°) and is positioned far away from the metal atoms. Finally, we included the pyracylenic [6,6] bond ***C*$_2$-A** situated close to one of the yttrium atoms (1.418 Å and 12.01°) (see Figure 7).

The C_2-C_{78} cage does not satisfy the IPR,[57] so it presents two adjacent pentagonal rings which have one yttrium atom directly facing them. Thus, all of the different types of C−C bonds ([6,6] types A, B, and C, [5,6] types D and F, and [5,5] type E; see Figure 1) can be found in this isomer. The Y_3N cluster remains planar when encapsulated in the C_2-C_{78} cage. Campanera et al.[10] made some predictions about the exohedral reactivity of another non-IPR endohedral derivative, $Sc_3N@C_2$-C_{68}, in which the [5,5] bonds were predicted to have a low reactivity on the basis of the Mayer bond order (MBO) analysis,[58] although they indicated that more detailed theoretical calculations were required to reach a definitive conclusion. To the best of our knowledge, the reactivity of the [5,5] bonds upon the Diels−Alder reaction has never been investigated in detail before.

As can be seen in Table 6, the Diels−Alder reaction over the [5,5] bond ***C*$_2$-E** of $Y_3N@C_2$-C_{78} is clearly favored, presenting an extremely exothermic reaction energy (−25.9 kcal mol^{-1}) in comparison with the other considered products. The non-IPR isomers are considered to be less stable than the IPR ones because of the presence of two abutted pentagons, which produces a severe steric tension that usually impedes the fullerene formation. In addition, two adjacent pentagonal rings lead to an eight-π-electron bicycle, which, according to the Hückel ($4n + 2$) aromatic/($4n$) antiaromatic rule, has a destabilizing effect over the π electronic structure.[57,59] As can be seen in Figure 7, [5,5] bonds have an yttrium atom directly facing toward them, and our previous results for $Y_3N@D_{3h}$-C_{78} have shown that the most stable addition is produced over a bond situated close to one of the yttrium atoms. Therefore, this reactivity preference for the addition close to the metal atoms might be dictated either by the encapsulated metal cluster or

(56) Greenwood, N. N.; Earnshaw, A. *Chemistry of the Elements*; Pergamon: Oxford, U.K, 1984.
(57) Kroto, H. W. *Nature* **1987**, *329*, 529–531.
(58) Mayer, I. *Chem. Phys. Lett.* **1983**, *97*, 270–274.
(59) Schmalz, T. G.; Seitz, W. A.; Klein, D. J.; Hite, G. E. *J. Am. Chem. Soc.* **1988**, *110*, 1113–1127.

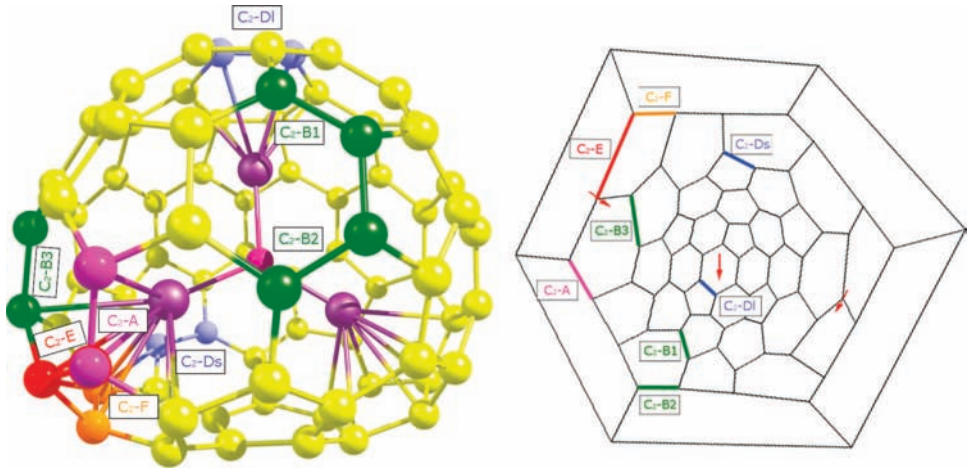

Figure 7. Various bonds of the $Y_3N@C_2$-C_{78} isomer selected for this study. Different colors are used to indicate the different bond types: pink, [6,6] type A; green, [6,6] type B; blue, [5,6] type D; red, [5,5] type E; orange, [5,6] type F. The Schlegel diagram, which converts the 3D structure into a 2D representation, is also shown. The positions of the yttrium atoms are marked using red arrows.

the fullerene cage. It is worth noting here that the distribution of charges in the carbon cage indicates that charge transferred from Y_3N to C_{78} does not lead to large accumulation of charge in any region of the fullerene (the largest difference between C atom charge in the $Y_3N@C_2$-C_{78} species is 0.04*e*). Actually, the more negatively charged carbon atoms are the ones situated close to the yttrium atoms ([5,5] and type-F [5,6] bonds), which, in contrast, have been shown to be the most reactive sites.

The second most stable addition is obtained when the cycloaddition reaction is produced again over the type-D [5,6] bond ***C_2*-Dl** (-10.3 kcal mol^{-1}), which is situated close to one of the yttrium atoms and exhibits the largest C−C bond distance (1.477 Å). This is in concordance with our previous results for the Diels−Alder reaction in the $Y_3N@D_{3h}$-C_{78} isomer. The addition of 1,3-butadiene over the type-F [5,6] bond ***C_2*-F** (which is not present in the IPR D_{3h} isomer because that isomer does not contain two abutted pentagon rings) also presents a moderate reaction energy (-8.4 kcal mol^{-1}). The rest of the bonds considered present reaction energies ranging from slightly exothermic to endothermic.

Effect of the Cluster Nature and Fullerene Strain on the Exohedral Reactivity of the C_2 Isomer of C_{78}. The highly favorable reaction energy found for the ***C_2*-E** adduct in the case of the Y_3N derivative could be mainly produced by the observed tendency for yttrium to react with those bonds situated close to it. Therefore, we also studied the Diels−Alder reaction for the free fullerene cage C_2-C_{78} and the scandium-based endohedral derivative $Sc_3N@C_2$-C_{78} over the same bonds that were investigated for $Y_3N@C_2$-C_{78}. Although the C_2 isomer is the most suitable cage for encapsulating the Y_3N cluster (the difference in energy between the C_2 and D_{3h} isomers is -20.2 kcal mol^{-1} at the BP86/TZP//BP86/DZP level), the C_2 isomer is not the most stable for C_2-C_{78} or $Sc_3N@C_2$-C_{78}, which are 70.5 and 37.8 kcal mol^{-1} less stable, respectively, than their corresponding D_{3h} isomers at the same level of theory.

The reaction energies of the Diels−Alder reaction on the free fullerene C_2-C_{78} cage and $Sc_3N@C_2$-C_{78} are reported in Table 6 and Figure 8. Interestingly, for all of the bonds studied, C_2-C_{78} is more reactive than $Sc_3N@C_2$-C_{78}, which in turn is more reactive than $Y_3N@C_2$-C_{78}. The only exceptions are, as in the D_{3h}-C_{78} cage, the two C−C bonds that have the longest bond lengths and are close to the yttrium atoms (***C_2*-B3** and ***C_2*-Dl**),

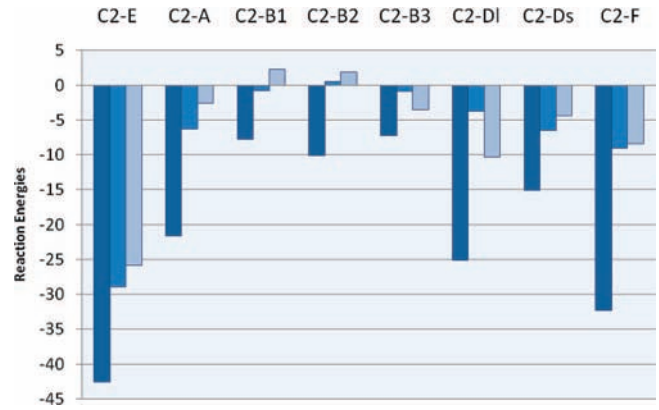

Figure 8. Comparison of the reaction energies (in kcal mol^{-1}) found for the Diels−Alder reaction over the selected bonds of the free C_2-C_{78} cage (dark blue), $Sc_3N@C_2$-C_{78} (blue), and $Y_3N@C_2$-C_{78} (light blue).

for which the reactivity increases in going from $Sc_3N@C_2$-C_{78} to $Y_3N@C_2$-C_{78}.

The cycloaddition reaction over the type-E [5,5] bonds is also extremely favorable in both cases (-42.6 and -28.9 kcal mol^{-1} for free C_2-C_{78} and $Sc_3N@C_2$-C_{78}, respectively). Therefore, the most important factor that contributes to the exohedral reactivity of the C_2 cage is not the nature of the encapsulated cluster but rather the fullerene strain energy. The regioselectivity of the exohedral functionalization in C_2-C_{78} is thus clearly dictated by the fullerene cage and is hardly modified by the endohedral cluster. The Diels−Alder reaction on the free C_2 cage and also on its scandium- or yttrium-based endohedral derivatives is extremely regioselective, as in all of the cases considered the reaction over the same type-E [5,5] bonds is clearly much more favorable. On the basis of these results, we might expect that the Diels−Alder reaction on other C_2 TNT endohedral metallofullerenes that have already been synthesized (such as $Tm_3N@C_2$-C_{78}[55] and $Dy_3N@C_2$-C_{78}[13]), might lead to the same [5,5] adduct.

The second most stable addition is produced over the considered type-F [5,6] bonds (situated next to the [5,5] junction) in either the free cage or the scandium endohedral fullerene, with reaction energies of -32.4 and -9.0 kcal mol^{-1}, respec-

tively. Recently, Lu et al.[60] investigated carbene addition on another non-IPR compound, $La_2@D_2$-C_{72}, and found that [5,5] bonds are less reactive than the adjacent type-F [5,6] ones. Although in our case of the Diels–Alder reaction, the type-F [5,6] bonds are less reactive than the [5,5] bonds, the attack over them leads to the second most stable addition for $Sc_3N@C_2$-C_{78} and C_2-C_{78} and to the third most favorable addition in the case of $Y_3N@C_2$-C_{78}. Thus, the finding of Lu et al. is in concordance with our results showing that the exohedral reactivity is clearly dependent on the fullerene strain of the studied cage (and in the case of the non-IPR structure C_2-C_{78} studied here, the encapsulated cluster hardly affects the fullerene reactivity).

Remarkable exothermic energies are also obtained for the addition over the type-D [5,6] bond ***C*$_2$-Dl** and over the type-A [6,6] bond ***C*$_2$-A** of C_2-C_{78} (−25.1 and −21.6 kcal mol^{-1}, respectively). It is interesting to note that although there is another type-D [5,6] bond (***C*$_2$-Ds**) that presents a shorter C−C bond distance (1.434 Å) than the one found in ***C*$_2$-Dl** (1.444 Å), the reaction is 10 kcal mol^{-1} more favorable for the latter, which is situated in this more deformed area close to the [5,5] bond region (θ_p = 9.75° for ***C*$_2$-Ds** and 12.20° for ***C*$_2$-Dl**; see Table 5 and Figure 8). The pyracylenic [6,6] bond ***C*$_2$-A** is also situated close to this more strained area (θ_p = 12.01°). Among the bonds considered, the type-B [6,6] bond ***C*$_2$-B3** is also close to the [5,5] junction (11.37°), but the reaction over it is clearly much less favorable (−7.2 kcal mol^{-1}). This is in concordance with what we found for the D_{3h}-C_{78} cage, where the reaction is clearly more favorable over the type-D [5,6] bond **b** and the pyracylenic [6,6] bonds **1** and **7**.

In the case of $Sc_3N@C_2$-C_{78}, the additions over the shortest [5,6] bond (***C*$_2$-Ds**, 1.418 Å) and the shortest [6,6] bond (***C*$_2$-A**, 1.405 Å) considered here lead to moderate exothermic reaction energies (−6.5 and −6.3 kcal mol^{-1}, respectively). The rest of the [5,6] and type-B [6,6] bonds studied here present slightly exothermic reaction energies. In contrast to the results obtained for the D_{3h} isomer, the type-B bonds situated far away from the scandium atoms with short bond distances and moderate pyramidalization angles do not present favorable reaction energies.

Conclusions

Our study of the Diels−Alder reaction on $Y_3N@D_{3h}$-C_{78} has shown that the most stable regioisomer is obtained when the attack is produced over a type-D [5,6] bond **d** that exhibits one of the longest C−C bond distances and a large pyramidalization angle. As far as we know, this is the first case of a cycloaddition reaction where the most stable addition is obtained over an extremely long C−C bond. This fact gives strong evidence that in fullerenes, not only short carbon bonds that exhibit more double-bond character can be quite reactive, but also those C−C bonds that present long distances that had classically been considered to be less or nonreactive. The unsuitable shape of the D_{3h} isomer for the encapsulation of bigger metal clusters such as Y_3N leads to a pyramidalization of the nitrogen atom. In this situation, the Y_3N unit is no longer planar, which produces two clearly differentiated areas. We have seen that there are only minor differences between the *up* region (which is close to the lone-pair electrons of the nitrogen atom) and the *down* area (which is much more affected by the yttrium atoms) considered in this study, except for bond **e**.

The regioselectivity of the exohedral addition is extremely modified by changing the nature of the cluster encapsulated inside: the most stable adduct for D_{3h}-C_{78} is obtained when the reaction occurs at the type-D [5,6] bond **b**, whereas in the case of $Sc_3N@D_{3h}$-C_{78} and $Y_3N@D_{3h}$-C_{78}, the type-B [6,6] bond **6** (situated far away from the scandium atoms) and the type-D [5,6] bond **d** (which is close to one of the yttrium atoms), respectively, are the most favored. This preference for reacting with those bonds situated close to the yttrium atoms is due to two different factors: first, the D_{3h} cage is extremely deformed, especially in the areas situated close to the yttrium atoms (which contain the most reactive bond **d**), so the attack reduces the strain energy of the cage; second, during the cycloaddition the Y_3N cluster gets additional space to adopt a more planar configuration.

The study of the Diels−Alder reaction on the most suitable cage for encapsulating the large Y_3N cluster, i.e., the C_2-C_{78} cage, has shown that type-E [5,5] bonds are by far the most reactive sites for the cycloaddition reaction. Moreover, we have found that these bonds are also the most reactive sites in both the C_2-C_{78} and the $Sc_3N@C_2$-C_{78} molecules. Therefore, it seems quite clear that the most important factor that contributes to the exohedral reactivity of the C_2 isomer is the fullerene strain energy and not the nature of the encapsulated cluster. On the basis of these results, we might expect that the Diels−Alder reaction over other C_2 TNT EMFs that have already been synthesized (such as $Tm_3N@C_2$-C_{78}[55] and $Dy_3N@C_2$-C_{78}[13]) might lead to the same [5,5] adduct.

Acknowledgment. This study was financially supported by the Spanish research projects CTQ2005-08797-C02-01/BQU and CTQ2008-03077/BQU, DURSI Project 2005SGR-00238, and MEC Fellowship AP2005-2992. The authors acknowledge the computer resources, technical expertise, and assistance provided by the Barcelona Supercomputing Center, Centro Nacional de Supercomputación.

Supporting Information Available: Pyramidalizations of the N atom in the $Y_3N@D_{3h}$-C_{78}−C_4H_6 adducts (Table S1); reaction energies of the methylene addition to selected bonds of $Y_3N@D_{3h}$-C_{78} (Table S2); deformation energies in the TSs for the different attacks of 1,3-butadiene on $Y_3N@D_{3h}$-C_{78} (Table S3); representations of the LUMO+7 (2) and LUMO+9 orbitals that present orbitals on bonds $\mathbf{e_u}$ and $\mathbf{e_d}$ suitable for interaction with the HOMO of the diene (Figure S1); BP86/DZP-optimized Cartesian *xyz* coordinates (Å) for all of the analyzed species (Table S4); and complete ref 33. This material is available free of charge via the Internet at http://pubs.acs.org.

JA8048783

(60) (a) Lu, X.; Nikawa, H.; Nakahodo, T.; Tsuchiya, T.; Ishitsuka, M. O.; Maeda, Y.; Akasaka, T.; Toki, M.; Sawa, H.; Slanina, Z.; Mizorogi, N.; Nagase, S. *J. Am. Chem. Soc.* **2008**, *130*, 9129–9136. (b) Lu, X.; Nikawa, H.; Tsuchiya, T.; Maeda, Y.; Ishitsuka, M. O.; Akasaka, T.; Toki, M.; Sawa, H.; Slanina, Z.; Mizorogi, N.; Nagase, S. *Angew. Chem., Int. Ed.* **2008**, *47*, 8642–8645.